THE JOURNAL OF PHYSICAL CHEMISTRY A LETTERS

2009, *113,* 791–796
Published on Web 01/09/2009

First Principles Study on the Diffusion of Alkali-Metal Ions on the Armchair Single-Wall Nanotubes

Jiong Li,[†] Haiming Li,[†] Xianqing Liang,[†,‡] Shuo Zhang,[†,‡] Ting Zhao,[†] Dingguo Xia,[∥] and Ziyu Wu*[,†,‡,§]

Beijing Synchrotron Radiation Facility, Institute of High Energy Physics, Chinese Academy of Sciences, Beijing 100049, People's Republic of China, National Synchrotron Radiation Laboratory, University of Science and Technology of China, Hefei 230026, People's Republic of China, Theoretical Physics Center for Science Facilities, Chinese Academy of Sciences, Beijing 100049, People's Republic of China, and College of Energy and Environmental Engineering, Beijing University of Technology, Beijing 100022, People's Republic of China

Received: October 07, 2008; Revised Manuscript Received: November 12, 2008

In this paper we have performed density-functional study on the adsorption and diffusion of various alkali-metal ions on the surface of pristine and defective armchair single-wall carbon nanotubes. In the pristine SWNT system, the position above the hexagon is believed to be the most stable site for adsorption, while the adsorption is enhanced in the defective SWNT. In pristine SWNT all the ions prefer to diffuse along the axial direction, with low barriers less than 0.25 eV. In defective SWNT, the axial diffusion is also energetically most preferable, and the barriers increase only slightly and have little influence on the diffusion as compared to pristine SWNT.

Introduction

Single-walled carbon nanotube (SWNT) possesses ideal physical and chemical properties, such as high stiffness, high thermal and chemical stability, and excellent conductance and transport property, etc. With these novel properties, SWNT has attracted much interest. Due to the large surface area of SWNT, many researches have been focused on the interaction between SWNT and various atoms, molecules, and groups, like alkali metals,[1−3] transition metals,[4,5] gas molecules,[6−8] DNA molecules,[9,10] etc. Among these studies, the alkali metals are particularly important, since they as well as SWNT are believed to show great potential for electrode materials.[11,12] Therefore, an in-depth study of the interaction between SWNT and alkali metals is of great significance.

Previous studies have shown that alkali-metal atoms prefer to be adsorbed on SWNT and the adsorption is dependent on the diameter of the nanotubes.[1] Within the process where the alkali-metal atoms penetrate the sidewall and intercalate into the internal nanotubes, they will encounter large barriers, which prevent them outside the pristine nanotubes at ambient temperature.[13] Nevertheless, most of these studies have been focused on the process of adsorption and intercalation, and there is still a lack of study on the surface diffusion of alkali metals on the SWNT. Furthermore, these studies mostly consider the neutral atomic state of alkali metals and in practice the alkali metals diffuse between the positive and negative electrodes in the ionic state. Thus a systematic study about surface diffusion of alkali-metal ions on SWNT is necessary.

In this work, we will systematically compare the adsorption and diffusion of three types of alkali-metal ions ($Li^+/Na^+/K^+$) on the external surface of armchair SWNT within density-functional calculations. First, we will compare the adsorption ability of these alkali-metal ions. Next, we will calculate their diffusion path on the surface of pristine SWNT and compare the barriers. Finally, we will consider their diffusion on the surface of defective SWNT. These results will help to further understand the diffusion mechanism of alkali metals on SWNT.

Method

In this study we performed density-functional calculations using B3LYP[14,15] as exchange-correlation functional, which has been widely used and proved to be accurate enough for extensive systems. All the calculations were performed by using the standard all-electron basis set 6-31G* within the Gaussian03 package. A finite-length armchair SWNT, which is denoted by the chiral index (5,5), was selected for study. All the dangling carbon atoms were passivated by hydrogen atoms (see Figure 1). Geometries are optimized to the default criterion.[16] To make a better compromise between the computational effort and the molecular model, we tested several SWNTs with the tubule length increasing from 7-layers to 15-layers and compared the results. We find that while the length is beyond 11-layers, the adsorption energy and local structure around the ions exhibits only a slight difference by reason that the interaction is short-ranged and mainly localizes between the adsorbed ions and their neighboring carbon atoms (will be mentioned below). Thus a SWNT with the length of 11-layers is considered to be accurate enough for our study.

* Corresponding author. E-mail: wuzy@ihep.ac.cn.
[†] Beijing Synchrotron Radiation Facility, Institute of High Energy Physics, Chinese Academy of Sciences.
[‡] National Synchrotron Radiation Laboratory, University of Science and Technology of China.
[∥] College of Energy and Environmental Engineering, Beijing University of Technology.
[§] Theoretical Physics Center for Science Facilities, Chinese Academy of Sciences.

10.1021/jp8088534 CCC: $40.75

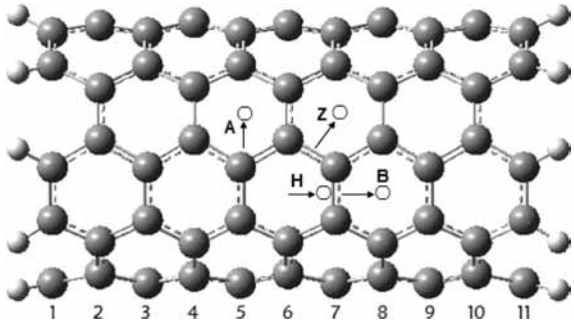

Figure 1. Schematic description of different adsorption sites in a 11-layers (5,5) SWNT.

We arrange the context as follows: first, the geometry of pristine (5,5) SWNT was fully optimized. Then alkali-metal ions were added on different sites on the surface of the SWNT to study the adsorption property. While the calculations of potential energy curves (PEC) along the directions between equivalent minimums were carried out, the structure of the SWNTs was fixed as the optimized result (the rationality will be mentioned below) and the height of the ions from the surface was optimized.

Results and Discussion

1. Adsorption of Alkali Metals on Pristine (5,5) SWNT Surface. To find the most stable site for adsorption, we choose several different sites: site H above the hexagonal ring, sites B and Z above the circular and zigzag C−C bonds, and site A above the carbon atom. All these structures with alkali metal adsorbed are fully optimized and the calculated adsorption energy, average interatomic distance from neighboring carbon atoms, and the NBO charge of adsorbed ions were listed in Table 1.

From Table 1 we could find that the hexagonal site is energetically the most stable site for adsorption for all three alkali-metal ions. Among these ions the Li^+ has the best ability to be adsorbed, with the shortest interatomic bond length, while K^+ has the weakest ability, with the longest interatomic bond length. Note that the intertube distance of SWNT bundles is about 5 Å, Li^+ could be easily intercalated into the interstitial space, while Na^+ and K^+ would encounter some repulsion due to their larger equilibrium distance from the surface.

TABLE 1: Calculated Adsorption Energy, Average Interatomic Distance, and NBO Charge Population of $Li^+/Na^+/K^+$ [a]

	E_{ads} (eV)	ion-C (Å)	NBO charge
Li^+-SWNT(H)	2.40	2.366	0.952
Li^+-SWNT(B)	2.14	2.174	0.959
Na^+-SWNT(H)	1.74	2.757	0.962
Na^+-SWNT(B)	1.60	2.527	0.965
K^+-SWNT(H)	1.22	3.180	0.976
K^+-SWNT(B)	1.14	2.955	0.977

[a] The Z and A sites are found unstable and will move to the H site.

During the adsorption process, all the ions have exhibited electron-withdrawing capability and accept a partial electron from the SWNT. The largest charge transfer occurs between SWNT and Li^+, indicating that the interaction is the strongest. This is consistent with the energy calculations, since the interaction is largely dependent on the charge transfer. The highest occupied molecular orbital (HOMO) as well as the lowest unoccupied molecular orbital (LUMO) of the SWNT are plotted in Figure 2. The HOMO and LUMO of pristine SWNT are occupied by the π and π^* orbitals which show delocalized property and are uniformly distributed over the hexagonal network. When the alkali-metal ion is adsorbed, the delocalized distribution is disturbed and the variation mainly localizes around the adsorbed ion, indicating that the interaction is short-ranged. Thus our finite cluster model is believed to have enough accuracy to simulate the infinite nanotube and to eliminate the effect of the edges.

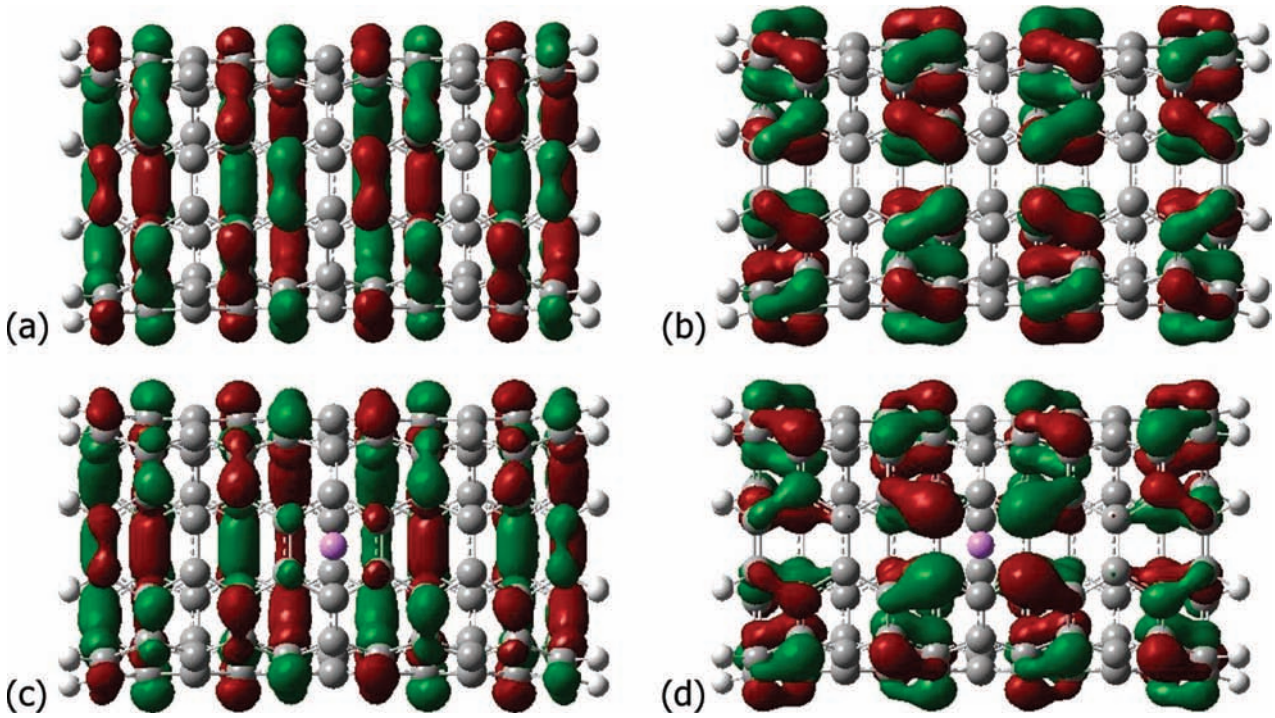

Figure 2. The HOMO of (5,5) SWNT (a) without and (c) with Li^+ adsorbed as well as the LUMO of (5,5) SWNT (b) without and (d) with Li^+ adsorbed.

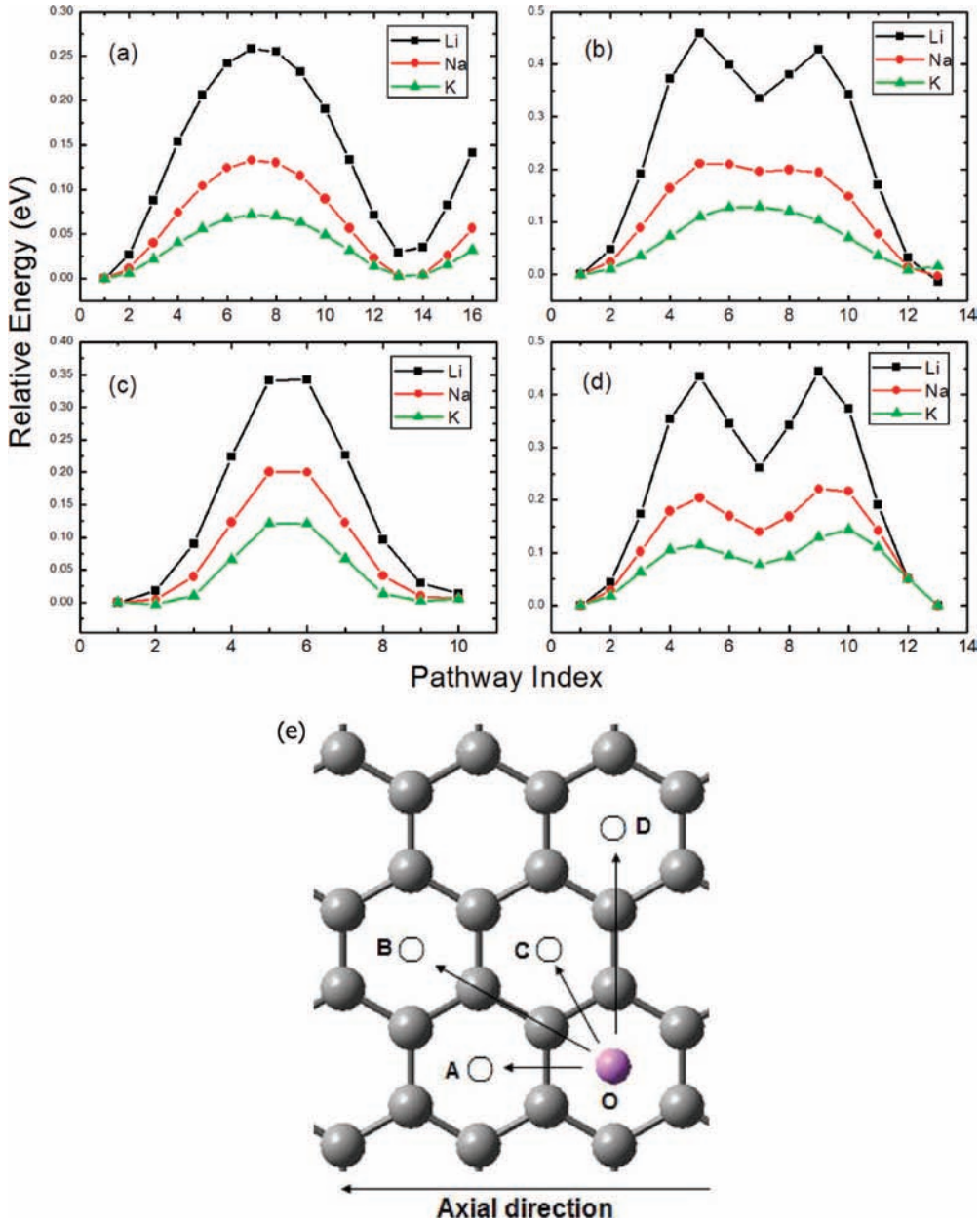

Figure 3. (a−d) Potential energy curves along different pathways as indicated in part e: (a) O → A; (b) O → B; (c) O → C; and (d) O → D.

Here, we should note that the above result is just a relative comparison and the interaction is actually somewhat weak, since the charge transfer is very small (less than 0.05e) and the geometry structure of the SWNT is only slightly changed by the adsorption, which is different from some other atoms, like hydrogen atoms which pull the carbon atoms out of the sidewall surface and form strong sp^3 hybridization.[7] Therefore, in the following calculations of diffusion, we will fix the SWNT as the optimized structure to preserve the original symmetry of the nanotube, which is believed to have enough accuracy, as well as to maintain the neighboring equivalence compared to the infinite nanotubes.

2. Diffusion of Alkali Metals on Pristine (5,5) SWNT Surface. When the alkali-metal ions diffuse on the surface of the SWNT, they are supposed to jump between minimums, which are supposed to be equivalent sites. From this point of view, there are three different groups of diffusion direction (see Figure 3a): straight direction along the axis (O → A), spiral direction surrounding the sidewall (O → B, O → C), and circular direction around the sidewall (O → D). When we calculate the PECs, we use the optimized SWNT as the substrate, and the height of the ions from the surface is optimized, with the ions relaxed perpendicular to the surface. The PECs along these pathways are plotted in Figure 3c−f. From the calculated PECs of different pathways, two features could be found.

First, the energetically most preferable pathways of the alkali-metal ions is in the axial direction (O → A). When the ions diffuse along the axial path O → A, an obvious barrier is observed, which corresponds to the saddle point above the C−C bridge site. The heights of the barriers are 0.26, 0.13, 0.08 eV respectively for Li^+, Na^+, K^+. But for the nonaxial pathways, the encountered barriers become higher. In the pathway from O to B, which corresponds to a helix angle of 30°, the barriers are 0.46, 0.21, and 0.13 eV, respectively. Moreover, in the pathway from O to C, which corresponds to a helix angle of 60°, the barriers are 0.34, 0.20, and 0.12 eV, respectively. As far as the circular diffusion (O → D) is concerned, the barriers are 0.44, 0.20, and 0.12 eV, respectively. The higher barriers in these nonaxial pathways are attributed to the unstable site, such as site A and site Z as indicated in Figure 2. These sites

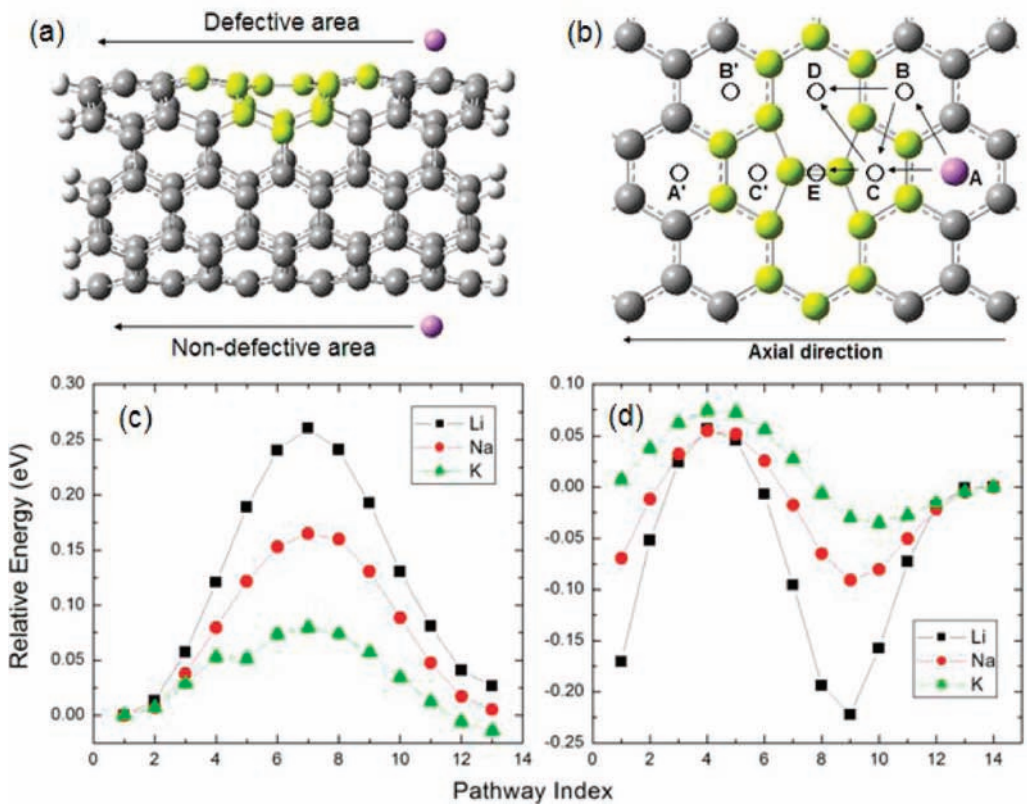

Figure 4. Schematic description of (a) Stone−Wales defect (yellow) and (b) different diffusion pathways; potential curves along the diffusion paths in (c) the nondefective area and (d) the defective area.

are energetically much more unstable than the bridge site above the circular C−C bond, thus leading to higher barriers and the two-peak shape of the PECs (as seen in Figure 3, parts d and f, except that in part d, K^+ exhibits only one peak, which we ascribe to the much smoother potential surface, and our computational method in this model could not distinguish the slight difference of less than 0.01 eV). We should mention that our result for Li^+ is much larger than that for lithium atom in the SWNT nanorope (47 meV) obtained by ab initio study.[13] The reason may be that we do not take into account the interaction between adjacent tubes; also the adsorption energy of lithium atom is much smaller than that of Li^+, which would lead to a small barrier.

Second, similar to the trend of adsorption energy, the diffusion barrier decreases as the atomic number increases. The strongest adsorption of Li^+ makes it possess a larger barrier than others, whereas the Na^+ and K^+ show very smooth potential curves along the diffusion pathway. However, the low barriers (less than 0.26 eV) ensure that the ions could easily diffuse along the axial direction. Note that while the concentration of adsorbed ions is increased, the average adsorption energy per ion will decrease. This is because the nearly completely positively charged alkali-metal ions will undergo strong repulsion from other ions, which will greatly reduce the adsorption energy. Therefore, Li^+ should be the better candidate for an ion battery with a better combination of adsorption and diffusion ability.

3. Adsorption and Diffusion of Alkali Metals on Defective (5,5) SWNT Surface. The above discussions are based on the pristine SWNT. Usually the SWNT is prepared with local defects (average ~2%[17]), such as carbon atom vacancy, interstitial carbon atom, Stone−Wales (SW) defect, etc. The existence of these defects may have an influence on the diffusion of alkali-metal ions and thus should be taken into account. In this section we will study SW defects to illustrate how the defects influence the diffusion of alkali-metal ions.

The SW defect can be generated topologically by rotating a C−C bond by 90° with respect to the midpoint of the bond. The geometry structure of SW along the axial direction could be seen in Figure 4a,b. The sidewall surface of a SW defective SWNT could be divided into two parts: the defective area (shown in yellow in Figure 4) and the nondefective area. When $Li^+/Na^+/K^+$ are adsorbed above the SW C−C bond (site E), the adsorption energies are 2.41/1.83/1.35 eV, respectively. Also, charge transfer occurs and the NBO populations on the adsorbed ions are 0.944/0.957/0.968, respectively. These adsorption energies and charge transfer values are larger than that of alkali-metal ions adsorbed on pristine SWNT, indicating that the distorted 7−7 ring fusion has stronger reactivity than pristine hexagon or the C−C bond.

From the frontier molecular orbital (MO, Figure 5a−d), we could see that the HOMO mainly localizes around the defective area, especially at the neighboring pentagons and heptagons of the rotated C−C bond. On the contrary, the LUMO shows similar delocalization behavior to the pristine SWNTs and distributes over the sidewall network uniformly. Furthermore, we consider the site projected DOS (PDOS)[18] of the Stone−Wales defect near the Fermi level (Figure 5e). For the PDOS of the two atoms in the rotated C−C bond, the energy of occupied states moves up to higher levels and the unoccupied states remain almost unchanged from the original energy level, as compared to the pristine SWNT, while for the other 14 atoms in the 5−7−7−5 rings, partial electronic states move to higher energy levels, for both occupied and unoccupied states. These results indicate that the Stone−Wales defects behave like an electron donor as compared to pristine SWNT. Therefore we could infer that for molecules and groups with high electrone-

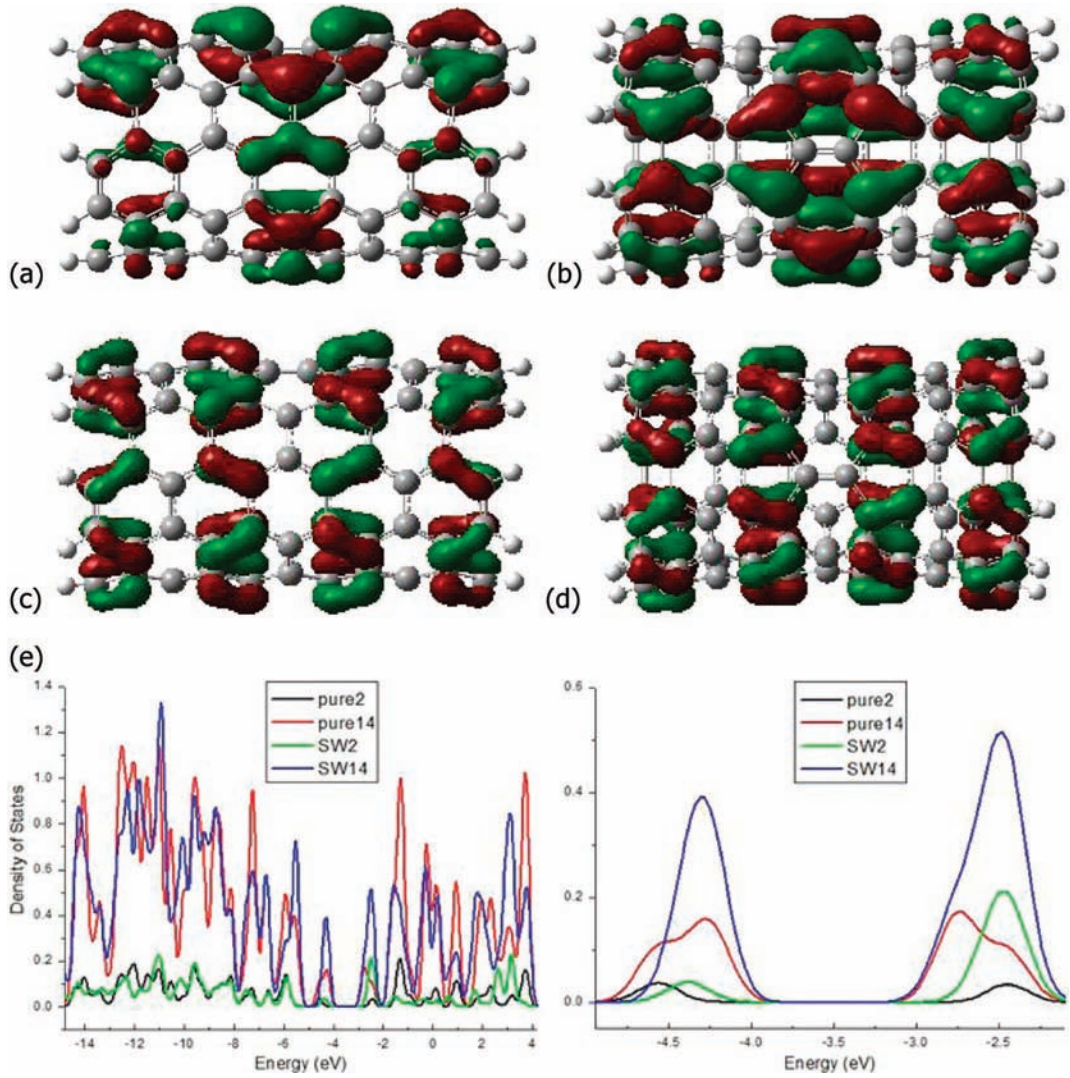

Figure 5. (a−d) HOMO and LUMO of Stone−Wales defective (5,5) SWNT: (a) side view and (b) top view of HOMO; (c) side view and (d) top view of LUMO. (e) PDOS of pristine and defective SWNT. Pure 2 and SW 14 denote the C−C bond and the other 14 carbon atoms in the pristine 6−6−6−6 and defective 5−7−7−5 ring fusion, respectively.

gativity, the Stone−Wales defects show stronger adsorption ability than pristine SWNT; but for molecules and groups with low electronegativity, the effect is not so obvious. This could explain why Stone−Wales defects show stronger reactivity when interacting with alkali-metal ions.

In Stone−Wales defective SWNT, there are more possible paths for diffusion. First we study the diffusion in the nondefective area to illustrate the effect of SW defects. We calculate the axial diffusion of alkali-metal ions on the opposite side of the nanotube, where the hexagonal network is less destroyed. The result is shown in Figure 4c and we could see that the diffusion barriers and the shape of the potential curves are nearly unchanged compared to those of pristine SWNT, indicating that the SW defects have little influence on the diffusion in the nondefective area. Therefore, only the defective area needs to be considered.

As far as the defective area is concerned, several possible positions around the SW defect for adsorption are selected. These positions are marked A, B, C, D, and E, as indicated in Figure 4a. Due to the mirror symmetry, their counter-sites are marked A′, B′, and C′, respectively. Therefore, there are several different pathways between site A and site A′, such as:

$$A \rightarrow C \rightarrow E \rightarrow C' \rightarrow A'$$
$$A \rightarrow B \rightarrow D \rightarrow B' \rightarrow A'$$
$$A \rightarrow C \rightarrow D \rightarrow C' \rightarrow A'$$

From our calculations, we find that the axial direction (A → C → E) is still the most energetically preferable pathway for diffusion, with the lowest barriers. Other pathways, such as A → B and C → D, having much higher barriers due to the local distortion, will prevent the diffusion. The potential curves of A → C → E are plotted in Figure 4d. In the pathway the first position is a local minimum (site A) and the maximum point at the fourth position corresponds to a saddle point, which locates above the C−C bond between the pentagon and hexagon. Then there is a descent in the energy and the ninth position becomes a minimum, which corresponds to the stable site above the pentagon ring (site C). From the pentagon to the SW C−C bridge site, the energy rises as interpreted by MO before. Note that in the PECs site A shows more stability than the SW C−C bond (site E), which seems to be contrary to our previous calculations. We ascribe this discrepancy to a change of the local structure of site A. The position is neighboring to the SW defect and the hexagon is actually affected and becomes more active than usual (see HOMO in Figure 5a,b). Moreover, site A is close to the edge of our finite-length tube, which also will enhance the activity. Therefore, during the diffusion the ions should stride over three barriers (A → C, C → E, C′ → A′), in which the barrier C′ → A′ is the largest. However, the values

are comparable to that of the pristine SWNT, which are 0.28, 0.15, and 0.11 eV, respectively. Thus the Stone−Wales defect seems to have little influence on the diffusion of alkali-metal ions. Other defects, like vacancy and interstitial, will be systematically studied later.

Conclusion

In this study, we have performed density-functional calculations on the adsorption and diffusion of alkali-metal ions on the external surface of armchair single-wall carbon nanotube. In pristine SWNT systems, all the ions prefer to be adsorbed above the hexagonal ring and Li^+ shows the strongest adsorption ability. When diffusing on the surface of pristine SWNTs, all the ions prefer to diffuse along the axial direction with a low barrier less than 0.25 eV. As far as Stone−Wales defects are concerned, they are believed to be more reactive than pristine SWNT. The axial diffusion is still the most energetically preferable, and the ions will encounter larger barriers, but the values of the barriers are comparable to the pristine SWNT and thus have little influence on the diffusion. From these results, we could get an in-depth understanding of the diffusion process of alkali-metal ions on the SWNT surface. SWNTs with different chirality, such as zigzag or chiral SWNTs, as well as their defective structures, will be systematically studied later.

Acknowledgment. This work is supported by the National Outstanding Youth Fund (Project No. 10125523 to Z.W.) and by the Knowledge Innovation Program of the Chinese Academy of Sciences (KJCX2-SW-N11). We would like to thank Prof. Jinlong Yang and Prof. A. Marcelli for the helpful advice and discussions.

References and Notes

(1) Udomvech, A.; Kerdcharoen, T.; Osotchan, T. First principles study of Li and Li^+ adsorbed on carbon nanotube: Variation of tubule diameter and length. *Chem. Phys. Lett.* **2005**, *406*, 161–66.

(2) Lugo-Solis, A.; Vasiliev, I. Ab initio study of K adsorption on graphene and carbon nanotubes: Role of long-range ionic forces. *Phys. Rev. B* **2007**, *76*, 235431–8.

(3) Zhao, M.; Xia, Y.; Mei, L. Diffusion and condensation of lithium atoms in single-walled carbon nanotubes. *Phys. Rev. B* **2005**, *71*, 165413–6.

(4) Durgun, E.; Ciraci, S. Spin-dependent electronic structure of transition-metal atomic chains adsorbed on single-wall carbon nanotubes. *Phys. Rev. B* **2006**, *74*, 125404–8.

(5) Yagi, Y.; Briere, T. M.; Sluiter, M. H. F.; Kumar, V.; Farajian, A. A.; Kawazoe, Y. Stable geometries and magnetic properties of single-walled carbon nanotubes doped with 3d transition metals: A first-principles study. *Phys. Rev. B* **2004**, *69*, 075414.

(6) Jiang, J.; Sandler, S. I. Nitrogen adsorption on carbon nanotube bundles: Role of the external surface. *Phys. Rev. B* **2003**, *68*, 245412.

(7) Lee, E.-C.; Kim, Y. S.; Jin, Y. G.; Chang, K. J. First-principles study of hydrogen adsorption on carbon nanotube surfaces. *Phys. Rev. B* **2002**, *66*, 073415.

(8) Sorescu, D. C.; Jordan, K. D.; Avouris, P. Theoretical Study of Oxygen Adsorption on Graphite and the (8,0) Single-walled Carbon Nanotube. *J. Phys. Chem. B* **2001**, *105*(45), 11227–32.

(9) Meng, S.; Maragakis, P.; Papaloukas, C.; Kaxiras, E. DNA Nucleoside Interaction and Identification with Carbon Nanotubes. *Nano Lett.* **2007**, *7*(1), 45–50.

(10) Zhao, X. C.; Johnson, J. K. Simulation of Adsorption of DNA on Carbon Nanotubes. *J. Am. Chem. Soc.* **2007**, *129*(34), 10438–45.

(11) Gao, B.; Bower, C.; Lorentzen, J. D.; Fleming, L.; Kleinhammes, A.; Tang, X. P.; McNeil, L. E.; Wu, Y.; Zhou, O. Enhanced saturation lithium composition in ball-milled single-walled carbon nanotubes. *Chem. Phys. Lett.* **2000**, *327*, 69–75.

(12) Gao, B.; Kleinhammes, A.; Tang, X. P.; Bower, C.; Fleming, L.; Wu, Y.; Zhou, O. Electrochemical intercalation of single-walled carbon nanotubes with lithium. *Chem. Phys. Lett.* **1999**, *307*, 153–157.

(13) Meunier, V.; Kephart, J.; Roland, C.; Bernholc, J. Ab Initio Investigations of Lithium Diffusion in Carbon Nanotube Systems. *Phys. Rev. Lett.* **2002**, *88*, 075506.

(14) Becke, A. D. Density-functional exchange-energy approximation with correct asymptotic behavior. *Phys. Rev. A* **1988**, *38*, 3098.

(15) Lee, C.; Yang, W.; Parr, R. G. Development of the Colle−Salvetti correlation-energy formula into a functional of the electron density. *Phys. Rev. B* **1988**, *37*, 785.

(16) The default convergence criterion in Gaussian03 is that the root mean square force, the maximum force, and the maximum displacement of atoms all have values smaller than 0.00030, 0.00120, 0.00045, and 0.00180 amu, respectively.

(17) Monthioux, M. Filling single-wall carbon nanotubes. *Carbon* **2002**, *40*(10), 1809–1823.

(18) Tenderholt, A. L.; Langner, K. M.; O'Boyle, N. M. A library for package-independent computational chemistry algorithms. *J. Comp. Chem.* **2008**, 839–845.

JP8088534